PCCP

Computational insights into lipid assisted peptide misfolding and aggregation in neurodegeneration

Journal:	*Physical Chemistry Chemical Physics*
Manuscript ID	CP-PER-05-2019-002765.R2
Article Type:	Perspective
Date Submitted by the Author:	27-Sep-2019
Complete List of Authors:	Sahoo, Abhilash; University of Maryland, Fischell Department of Bioengineering Matysiak, Silvina; University of Maryland, Fischell Department of Bioengineering

PCCP

ROYAL SOCIETY OF CHEMISTRY

ARTICLE TYPE

Cite this: DOI: 10.1039/xxxxxxxxxx

Computational insights into lipid assisted peptide misfolding and aggregation in neurodegeneration

Abhilash Sahoo,[a] and Silvina Matysiak[ab]*

Received Date
Accepted Date

DOI: 10.1039/xxxxxxxxxx

www.rsc.org/journalname

Peptide misfolding and aberrant assembly in membranous micro-environments have been associated with numerous neurodegenerative diseases. The biomolecular mechanisms and biophysical implications of these amyloid membrane interactions have been under extensive research and can assist in understanding disease pathogenesis and potential development of rational therapeutics. But, the complex nature and diversity of biomolecular interactions, structural transitions, and dependence on local environmental conditions have made accurate microscopic characterization challenging. In this review, using cases of Alzheimer's disease (amyloid-beta peptide), Parkinson's disease (alpha-synuclein peptide) and Huntington's disease (huntingtin protein), we illustrate existing challenges in experimental investigations and summarize recent relevant numerical simulation studies into amyloidogenic peptide-membrane interactions. In addition we project directions for future in-silico studies and discuss shortcomings of current computational approaches.

1 Introduction

Accumulation of proteinaceous amyloid-like aggregates is a recurrent theme in numerous diseases associated with neuronal dysfunction[1]. In particular, due to relatively higher and progressively increasing incidence, Alzheimer's, Parkinson's and Huntington's disease present a significant social and economic challenge. Despite variations in pathogenic peptide type and amino acid sequences, oligomeric-aggregates associated with these diseases share many common structural properties[2]. These amyloid fibrillar deposits/inclusions are often characterized by single-component-dominant, cross beta structures with beta sheets positioned perpendicular to fibril axis. While misfolded amyloid peptides can form mature fibrils and protofibrils through progressive self-association, an emerging body of evidence implicates smaller polymorphic pre-fibrillar, on-pathway and off-pathway oligomers as the primary toxic species[3–6]. A detailed understanding of the molecular mechanisms and pathological event pathways of early-stage amyloid oligomerization can aid towards development of rational therapeutics. Many common pathways for amyloid aggregation related cytotoxicity has been outlined — ionic homeostasis, mitochondrial dysfunction, altered signaling and autophagy. Many of these pathways involve extensive membrane-peptide interactions[7–10]. Moreover, membranes constitute a significant proportion of cytosolic components and the amphipathic nature of pathogenic amyloid peptides and aggregates can amplify toxic membrane associations and insertion.

Experimental investigations into structural features of amyloid oligomer-membrane interaction is limited due to extensive structural heterogeneity, complex competing interactions — membrane affinity & peptide aggregation and transient nature of oligomeric intermediates. Therefore, it is not possible to study this process using a single traditional biophysical techniques, which often provide spatio-temporally averaged information. Oligomer-membrane affinity and binding have been investigated through chromatography[11], centrifugation[12], density gradient techniques[13], infrared spectroscopy[14–16], mass spectroscopy[16], and surface plasmon resonance (SPR)[17,18]. Structural implications of oligomer/fibril-membrane interactions have been probed using black lipid membranes (BLM)[9,19,20], microscopy techniques (atomic force microscopy (AFM)[7,20], transmission electron microscopy (TEM)[21]), fluorescence microscopy[22,23], nuclear magnetic resonance (NMR)[24], electron paramagnetic resonance (EPR)[25,26] and circular dichroism (CD)[24]. On the other hand, studies have relied on fluorescence spectroscopy[27–30] to study kinetics and dynamics. Novel variations and combinations of aforementioned techniques have proved more successful in characterization of amyloid-membrane assemblies. Multiple possible structural mechanisms and models of membrane disruption (Figure 1) by oligomer-membrane interactions — membrane-pore model, carpeting model and detergent model have been proposed to explain experimental observations[31]. Although these

[a] Biophysics Program, Institute of Physical Science and Technology, University of Maryland, College Park, MD
[b] Fischell Department of Bioengineering, University of Maryland, College Park, MD. E-mail: matysiak@umd.edu

models provide possible descriptions of their respective experimental observations, the accurate characterization and pathways of membrane disruption is missing. In addition to diverging interpretations, the intrinsically disordered nature of aggregating peptides are highly susceptible to local environmental alterations and generate experimental artifacts which often remain unaccounted for, leading to controversial results.

Molecular simulations, aided by statistical thermodynamics complement and/or serve as surrogates for experiments by providing both atomic-scale structural and kinetic insights. The molecular and mechanistic details from in-silico observations can also assist therapeutic drug design. Classical molecular dynamics involves direct numerical integration of Newton's equations, aided by mathematical functions and parameters — *forcefield*, that describe the dependence of system's potential energy on individual atomic positions to generate time evolution of molecules[32]. It can be particularly ideal for characterizing transient oligomeric structures which are difficult to study experimentally and has been widely used to evaluate heterogeneous ensemble of structures generated by amyloid peptides. On the basis of particle-based resolution, molecular dynamics simulations can be broadly classified into all-atom (AA), united-atom (UA) and coarse grained (CG)[33]. The efficiency and accuracy of bio-molecular simulations is dependent on mathematical forcefields and packaged molecular dynamics simulation programs (GROMACS[34], CHARMM[35], NAMD[36] and DLPoly[37], etc.). Some of the popular chemically specific peptide-lipid forcefield families are Assisted Model Building and Energy Refinement[38,39] (AMBER), Chemistry at HARvard Molecular Mechanics[40–42] (CHARMM), GROningen MOlecular Simulation[43,44] (GROMOS), Optimized Potential for Liquid Simulations[45,46] (OPLS) and MARTINI[47,48] (a coarse-grained potential). Improvements in parallel computing architecture and use of graphical processing units have enabled millisecond level atomistic simulations to study protein folding and unfolding in an unbiased manner.

While atomistic simulations provide higher resolution and more detailed insights about the peptide-membrane biomolecular systems, the spatio-temporal scales to study large-scale oligomerization and oligomer-lipid interactions cannot be reliably achieved by present-day computational machineries. On the other hand, due to fewer number of particles — resulting in lowered resolution and a smoother free-energy landscape, coarse grained (CG) MD can provide a more holistic picture for such multi-agent phenomena. Here we present a systematic survey of molecular dynamics simulations — atomistic and coarse grained to catalouge amyloid monomer/oligomer-membrane interactions in common neurodegenerative diseases — Alzheimer's (AD), Parkinson's (PD) and Huntington's disease (HD) to present a cohesive picture.

2 Alzheimer's Disease - Aβ peptides

Amyloid plaques and neurofibrillary tangles, contributing to progressive cognitive decline have been established as hallmarks for Alzheimer's disease[49–53]. The amyloid cascade hypothesis, has been widely accepted by neuropathologists as the primary model of AD pathogenesis. According to this hypothesis, oligomerization of Aβ peptides initiates a cascade of events, culminating in neuronal dysfunction and dementia[54–58]. Pathogenic Aβ peptides are about 39-43 residue (Figure 2a) long intrinsically disordered peptide in aqueous solution and ordered alpha helix rich structures in apolar environments (Figure 2b), formed from successive incisions by β–secretase and γ–secretase, which can aggregate into β–sheet rich aggregates. The interaction of these Aβ–oligomers with neuronal membranes can lead to significant membrane disruptions[59–65]. The interactions are highly heterogeneous with significant dependencies on membrane composition, oligomer structure, peptide/lipid ratio and cellular environment. We have curated a brief list of experimentally observed Aβ peptide-membrane interactions.

Aggregation kinetics was significantly altered in presence of brain total lipid extract (BTLE), with reduced lag-times and slower elongation rates as compared to aggregation in solution[66]. Importance of bilayer physical properties — surface charge, hydrophobicity and roughness in modulating Aβ-membrane interaction, was investigated using atomic force microscopy and membrane mimicking surfaces such as silica, mica, graphite and teflon[67–70]. These experiments reveal the prominent role of surface charge and electrostatic interaction between peptides and membrane in dictating peptide absorption and aggregation. Particularly, peptide-membrane binding and subsequent aggregation is weaker for 1-palmitoyl-2-oleoyl-*sn*-glycero-3-phospho-L-choline (POPC), compared to model membranes created from anionic lipids such as 1-palmitoyl-2-oleoyl-sn-glycero-3-phospho-(1'-rac-glycerol) (POPG)[71]. Beyond membrane composition induced surface charge, the presence of sterols which modulate membrane biophysical properties are an important part of membrane assisted Aβ aggregation.

On the other hand, studies have also supported a multi-modal form of Aβ monomer/oligomer assisted membrane disruption. Kayed *et. el.*[72] suggested increased membrane conductance as a consequence of membrane thinning due to asymmetric pressure from Aβ oligomer - bilayer surface interaction (carpeting model - Figure 1). Pore formation due to Aβ membrane interactions is evidenced from doughnut shapes in AFM and release of encapsulated fluorescent dyes from LUVs, leading up to ionic disbalance[7]. Moreover micelle-like behavior and subsequent lipid-extraction by Aβ oligomer has been hypothesized from the observation that a structurally similar peptide, IAPP disrupts membrane by reduction of membrane surface tension and consequent removal of lipids[73]. Quasi-elastic neutron scattering (QENS) studies have been extensively employed to study alterations in lipid dynamics in presence of Aβ peptides. Experiments by Barett *et. al.* reported a discrepancy in Aβ 22-40 induced lipid-lateral diffusion at different fluidity levels of a DMPC/DMPS membrane[74]. In gel state, Aβ peptide induced an increase in lateral diffusion, whereas there was a significant decrease in in-plane lateral diffusion in a more disordered state. Investigations by Buchsteiner *et. al.* also revealed an increase in lateral diffusion of DMPC/DMPS membrane in its liquid crystalline state on interacting with Aβ 25-35[75]. These works suggest a decrease in membrane stability and increased membrane fluidity induced by interaction with embeded Aβ peptide fragments. On the other hand, QENS studies

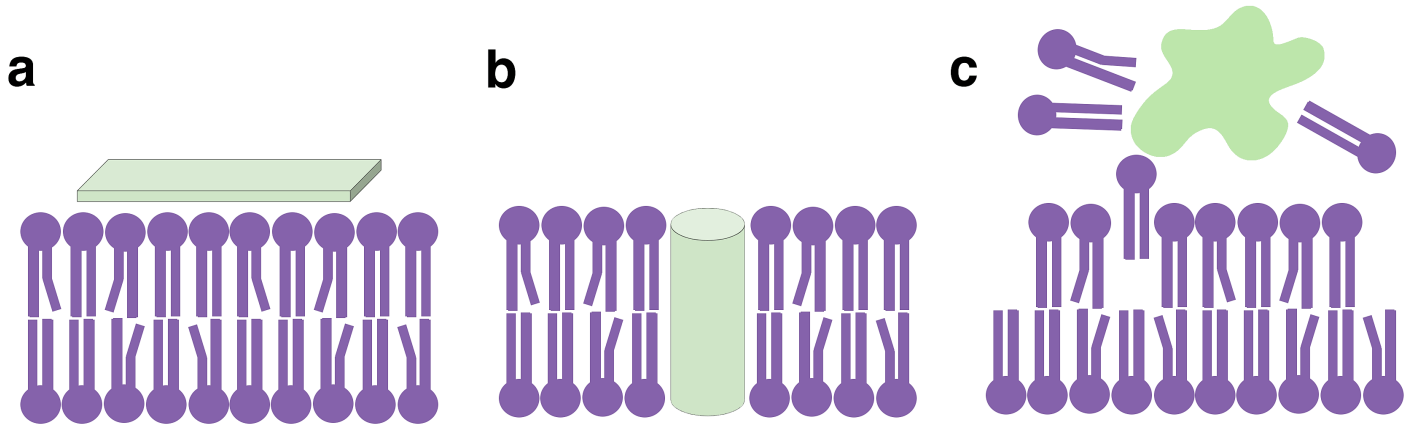

Fig. 1 Three modes of membrane disruption due to oligomer-membrane interactions. (**a**) **Carpeting model:** Accumulation of amyloid aggregates on membrane surface imparts unequal stress on bilayer, resulting in membrane disruption. (**b**) **Membrane-pore model:** Oligomers insert into the membrane creating membrane-pores that destabilizes ionic homeostasis. (**b**) **Detergent model:** Oligomers on interacting with a membrane can start a micelle-like effect and remove lipid molecules from the bilayer.

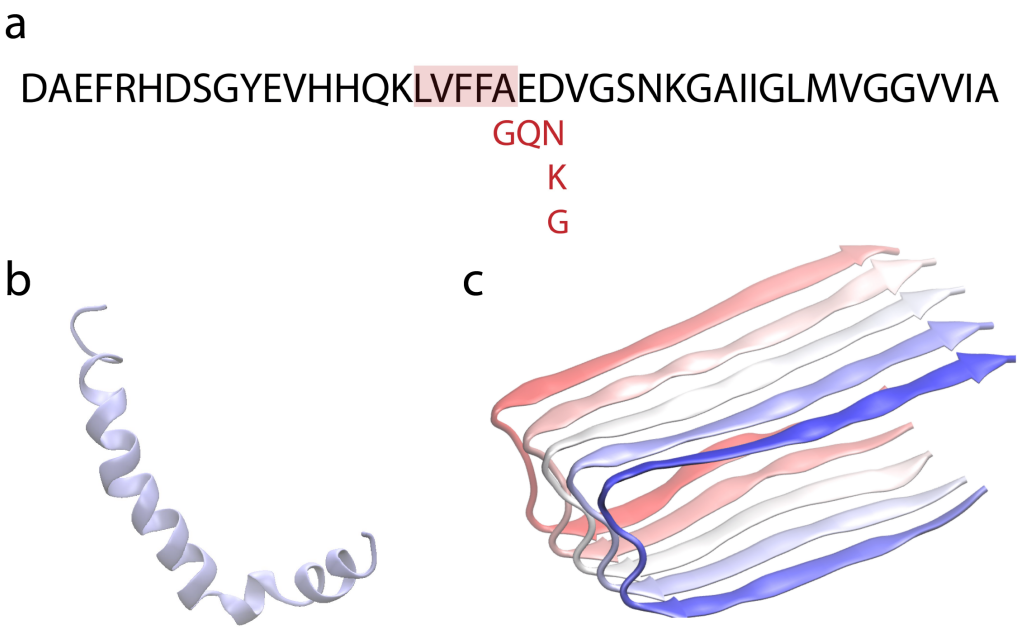

Fig. 2 a) Amino acids in Aβ 1-42 peptide. The red shaded region represents the central hydrophobic core and the characters in red are some of the familial mutants. b) In-solution structure of a single monomer in apolar micro-environment (pdb: 1IYT) c) A representative structure of Aβ oligomer (pdb: 2BEG) in solution. The aggregate is colored to distinguish peptide chains. Aβ oligomers are highly dynamic and can have different structure depending on local environmental changes.

by Rai *et. al.* using DMPG unilamellar vesicles and Aβ 1-40 peptides suggested an increase in lipid lateral diffusion in disordered phase with no appreciable changes in gel phase[76]. The effective thinning of DMPG bilayer on addition of Aβ peptide has been implicated for this increased lateral diffusion. The authors used small angle neutron scattering and neutron membrane diffraction to report that Aβ 1-40 bound strongly to DMPG headgroup and did not penetrate. This aforementioned works on lipid dynamics also presents evidence of how differential binding of Aβ peptide with lipid membranes, imposed by physical properties of lipids, can in turn affect lipid dynamics.

Considering the associated system size and numerical complexity, all-atom molecular dynamics simulations have predominantly focused on pre-inserted Aβ oligomer-membrane interactions, simulations with specific shorter peptide segments and enforced surface-bound interactions. Simulations with different explicit and implicit solvent forcefields, along with implementation of advances sampling techniques have been explored.

2.1 Aβ monomer/oligomers-membrane surface interaction

Atomistic molecular dynamics simulations using model zwitterionic (DPPC) and anionic (DOPS) membranes were recently

used to study Aβ dimerization on a membrane surface[77]. The authors used two different types of Aβ peptide — negatively charged (-3) for DPPC membrane and neutral for DOPS membrane to incorporate local pH alterations in presence of DOPS membranes. The simulations and thermodynamic cycle calculations predicted that irrespective of dimer's structure (β-hairpin or extended) there were stronger peptide-peptide interactions compared to peptide-lipid interactions for DOPS, actively promoting dimerization. These authors hypothesize the neutral Aβ peptide formed due to reduction in pH closer to PS membrane contributes to this effect. Stronger peptide-peptide interaction also presents a possibility of dissociation of peptide-dimer from lipid bilayer surface. Free energy perturbation calculations and Replica Exchange Molecular Dynamics (REMD), with GROMOS 53a6 force field, of Aβ 11-40 trimer suggested ease of trimer's membrane (DPPC) insertion and dominance of van-der Waals interactions over electrostatics in trimer-bilayer binding[78]. While the β sheet rich region remained completely buried into the lipid bilayer, the more disordered random coil region preferred to interact with lipid headgroup. Collision cross section (CCS), calculated using ion mobility projection approximation calculation tool[79] (IMPACT) suggested similar trimer CCS while solvated in solution and embedded in membranes. In contrast, CHARMM27 simulations of Aβ 17-42, β-strand-turn-β-strand pentamer (pdb code: 2BEG (Figure 2)) binding to charged - POPC/POPG and zwitterionic - POPC bilayers, suggests critical importance of electrostatics in this process[80]. The impact of bilayer composition induced membrane biophysical properties on monomeric Aβ peptide binding was investigated by Ahyayauch *et. al.*[81]. Their MD simulation studies with OPLS-AA and model lipid membranes composed of varying concentrations of PSM (N-palmitoylsphingomyelin) / DMPA (1,2-Dimyristoyl-sn-glycero-3-phosphate) / Cholesterol show although charged bilayer promote binding as compared to uncharged ones, the peptide-lipid contacts are more numerous in low-charged than high-charged bilayers. Although, the presence of DMPA (5 %) initiated a conversion to β sheet, the increase in concentration of DMPA (20 %) resulted in retention of initial α helical structure. In addition, their experimental studies present that binding of peptides to membranes in L_d (liquid disordered) state is stronger and less electrostatics-driven than L_o (liquid ordered) phase. Recently, differences between POPC and POPC-Cholesterol-PSM raft membranes with respect to $A\beta$ tetramer-membrane interactions were established by GROMOS-53a6 simulations[82]. The results depict higher insertion and successive disruption (predicted) of POPC bilayer compared to the model raft. This study presents a validation of carpeting model for membrane disruption. Slower self-diffusion of peptide-tetramers and increased elongation into rod-like structures in presence of lipid rafts were hypothesized as possible contributors towards experimentally observed increased fibrillation on raft membranes[83]. Davis *et. al*[84] used constrained (umbrella sampling) and unconstrained MD to characterize Aβ 1-42 interaction with DPPC and DOPS starting from helical, β-hairpin and random coil structures at multiple pH values using GROMOS96 force field. Peptides on DPPC have a more parallel structure, consequently maximizing peptide-membrane contacts as compared to DOPS, which promotes a more "superficial" and parallel orientation with N-terminal hydrophobic groups embedded into the bilayer. While interaction with PS membranes do not result in a stable secondary structure enriched monomeric conformation, it does stabilize transient states with high propensity for aggregation. Another study[85] by the same group using extensive REMD showed that the population of D23-K28 interaction that promotes β-hairpins is reduced in phospholipid bilayers, which promote interaction between K28 and phosphate. Hoshinho *et. al.*[86] measured adhesion and binding probabilities of Aβ 1-42 with membranes containing GM1 (ganglioside). The interaction of Aβ 1-42 with membrane is driven by interaction of GM1 with peptide aromatic residues and K28's amine group. They also reported sequential assembly of Aβ peptides and stronger peptide-peptide hydrophobic interactions capable of transiently removing assembled complex from membrane. The binding of monomeric Aβ to the membrane was established by interaction of K28 with neuraminic acids, leading to deformation and increased hydrophobic association of C-terminus with the membrane.

2.2 Aβ monomer/oligomers-membrane insertion and transmembrane interactions

Simulations of Aβ 1–42 with POPC, POPG and DPPC have revealed stability of monomers and oligomers embedded into membranes[87]. Zwitterionic membranes, tail unsaturation and peptide-oligomerization promoted stability of such transmembrane structures. The presence of transmembrane structures lead to enhanced water translocation, in a membrane dependent fashion. Implicit membrane simulation studies with basin-exchange parallel tempering have been employed to characterize stable transmembrane oligomer structures[88]. While, β sheet with a typical strand-turn-strand unit was found to be the most stable species for oligomers up to size six, octamers assembled into two distinct tetrameric units. Kargar *et. al.*[89] used OPLS-AA force field to observe relative stability of a part membrane-inserted (DPPC) Aβ 1-40 monomer across multiple temperatures. Insertion of peptides into the lipid bilayer was observed to increase with increasing temperature. In addition, strong interactions between inserted peptide and neighboring phospholipids imparted a tilt and increased fluidity to locally-close lipid molecules, resulting in membrane thinning.

All-atom simulations with GROMS96-53a6 force-field to study dimerization process of closely-placed and membrane-inserted Aβ 1-40 reveal that the aggregation process is led by the polar N-terminus residues[90]. Membranes of varying compositions behaved differently, with "strong" peptide assemblies and significant membrane disruption in POPC compared to "weak" peptide assemblies and stronger peptide-lipid interactions in POPS and POPE. The strength of peptide assembly (weak/strong) is inferred from geometry-based parameters — number of heavy atom contacts and separation of center of masses. Membrane disruption was particularly low in raft membranes (enriched with sphingomylin and cholesterol). Simulations by Jang *et. al.*[91] using CHARMM27, presented an unbiased and spontaneous insertion-pathway of truncated Aβ 17-42 into DOPC membrane, using a particular (U-shaped—β-strand-turn-β-strand (p3) pentameric

aggregate) conformation. The simulations revealed four distinct sequential steps characterizing the pathway for membrane insertion — "initial touch, partial deposition, oblique insertion and embedded oligomers". This study also reported that dimeric aggregates with a U-shaped motif in membranous environments were relatively less stable than pentameric ones, due to a disruption of β sheet contacts. CHARMM36 simulations of mixed lipid bilayer (POPC & DMPS) with pre-inserted Aβ 25-35 showed development of negative local membrane curvature[92]. In addition, the presence of membrane modulating drugs such as Curcumin, Acetylsalicylic acid (ASA) and Melatonin, which partitioned into lipid head-tail interface led to differential modulation of Aβ 25-35 aggregating behavior. While Melatonin did not affect Aβ 25-35 aggregation, the presence of ASA, that increases membrane stiffening, increased peptide aggregation. On the other hand Curcumin, which increased lipid surface area to create a softer and thinner membrane led to a decrease peptide aggregation. Poojari *et. al.* studied the effect of site-specific mutations (E22G - Arctic mutant, D23G - Arctic-type mutant, E22G/D23G, K16M/K28M and K16M/E22G/D23G/K28M) on transmembrane stability by using GROMOS96 simulations of POPC-inserted Aβ 1-42 peptides—monomers and tetramers[93]. The mutants were chosen to primarily investigate the effect of charged groups at the trans-membrane region in oligomer stability. While E22G Aβ_{42} demonstrated the highest stability, D23G showed relatively lower stability and significant membrane disruption. In general, all the site-specific mutants were similar or more stable than wild-type Aβ 1-42 peptides.

Qiu *et. al.* compared structural properties and transitions of partially inserted monomeric Aβ peptide in cholesterol depleted and enriched POPC membranes using GROMOS87[94]. Their simulations suggest a protective role of cholesterol by preventing structural transition — from α helix to β sheet and decreasing membrane disruption. While the smaller Aβ 1-40 preferred a partly inserted conformation, the longer and more hydrophobic Aβ 1-42 remained completely inserted in cholesterol enriched PC membrane. The presence of cholesterol resulted in approximately doubling the insertion efficiency of Aβ peptide. The authors also reported an increased membrane disruption due to inserted form of Aβ 1-40, compared to Aβ 1-42, possibly due to hydrophobic length mis-match of the larger peptide. Xiang et. al. investigated Aβ 11-42 peptide and oligomer interaction in POPC membranes with varying concentrations of cholesterol using CHARMM36 forcefield[95]. Both for monomeric and trimeric Aβ (S-shaped triple-β-strand) system, increase in cholesterol concentration, pushed the peptide/peptide-aggregate out from its pre-inserted initial state. The free energy profile of monomer insertion as a function of membrane's cholesterol content suggests ease of initial membrane adhesion and larger barrier to membrane insertion with increasing cholesterol concentration. The authors also reported easier peptide insertion in trimeric form as compared to monomers and possible water pore formation in N-terminal inserted Aβ 11-42 trimer. The protective role of cholesterol and displacement of sterols to facilitate oligomer membrane insertion has been established by many previous experimental observations[96,97]. This discrepancy in the two reported studies regarding Aβ membrane insertion may be associated with molecular dynamics forcefields and/or different lengths of peptide used. It is worth noting that recent studies have also reported enhanced Aβ peptide aggregation with increasing cholesterol content[98]. An accurate description of the influences of sterol content on Aβ-membrane interaction is still not available

Beyond traditional MD and advanced sampling methods, Monte Carlo (MC) and coarse-grained molecular dynamics (CG-MD) simulations are being used to address the long time and length scale issues of Aβ aggregation on membrane. Transmembrane stability of Aβ 1-42 and related familial mutants were tested by implicit-membrane Monte Carlo simulations[101]. Although the ease of membrane insertion was not different for wild type and familial/synthetic mutants, significant variations were reported in the pathway of insertion. The mutants, except for E22G favored a partially inserted conformation more than wild-type. Partial insertion of peptides was hypothesized as a potential reason for increased toxicity of familial and artificial mutants. Liguori *et. al.* investigated the impact of cholesterol asymmetry in modulating the extracellular release of Aβ 1-42 from a cell-like planar lipid bilayer using MARTINI simulations[102]. Multiple lipid bilayer systems were created with POPC, POPS, cholesterol and DOPE molecules with different concentrations at exofacial and cytofacial leaflets to generate this asymmetry while maintaining anionic nature of cytofacial leaflet. Increase in concentration of cholesterol in the exofacial leaflet promotes the extrusion of highly reactive N-terminal residues. In addition peptide-membrane simulations with two Aβ 1-42 conformations — 1IYT (α helix content of 70%) and 1Z0Q (α helix content of about 30%) showed that the increase in C-terminal helical content contributes to increased membrane retention. Multiscale simulations were employed to study pre-embedded (α helical) peptide aggregation in POPC lipid bilayer and its impact on bilayer structure[103]. First, coarse grained simulations with MARTINI forcefield was used to facilitate faster diffusion and aggregation of *A*β 1-40 peptide in POPC membranes. Then, the coarse grained structures were reverse-mapped to all-atom structures and simulated with GROMOS96 force field to study stability of secondary structures. While, high (1:36) peptide-lipid ratio favour large aggregations, smaller dimeric and trimeric aggregates are more favored in simulations with lower peptide concentrations. In addition, the 300 ns of all-atom study starting from reverse-mapped trans-membrane aggregate structure at the end of coarse grained simulation, confirms that the initial α helix structure is maintained through the simulation time. This work also proposed a geometry-based analytic framework to explain super-structures generated in simulations and the impact on membrane due to peptide aggregation. More recently our group used in-house developed membrane (WEPMEM)[100,104] and peptide (WEPPROM)[100,105] forcefields, that uses explicitly introduced structural polarization to reproduce accurate electrostatics (Figure 3), to study aggregation of the central hydrophobic core — Aβ 16-22 starting from a solvated state in presence of zwitterionic (POPC) and anionic (POPS) model membranes[99]. While, peptide self-association, facilitated primarily by diffusion was relatively faster in POPC, the emergence of ordered beta sheet rich

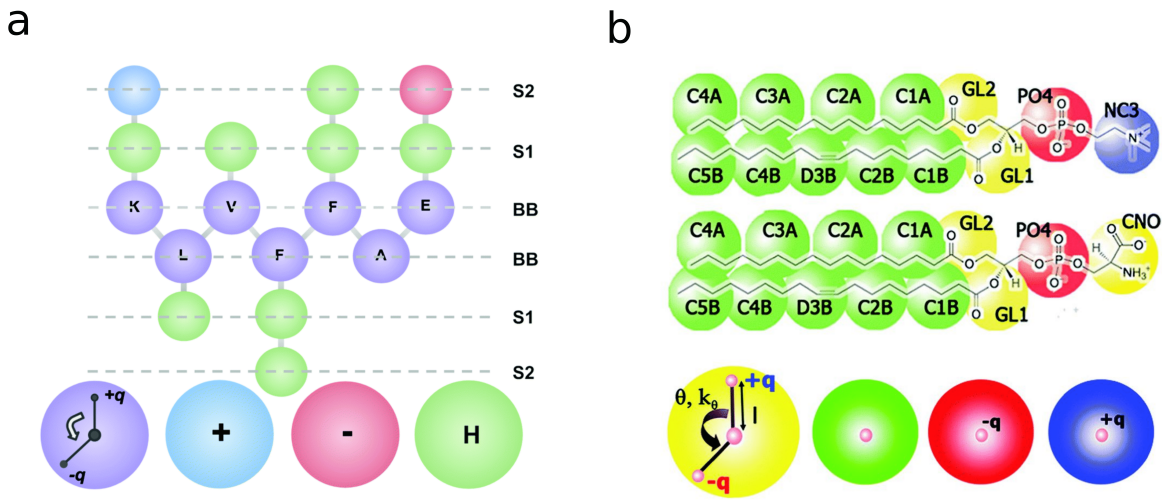

Fig. 3 a) Peptide - Water-Explicit Polarizable PROtein Model (WEPPROM) reproduced from Sahoo *et. al.*[99] b) Membrane - Water-Explicit Polarizable MEMbrane (WEPMEM) model reproduced from Ganesan *et.al.*[100] with permission from the PCCP Owner Societies. The partial charges on peptide backbone (violet) and polarizable beads (yellow) of lipids generate explicit structural polarization and provide directionality to dipolar interactions that can result in structural transitions.

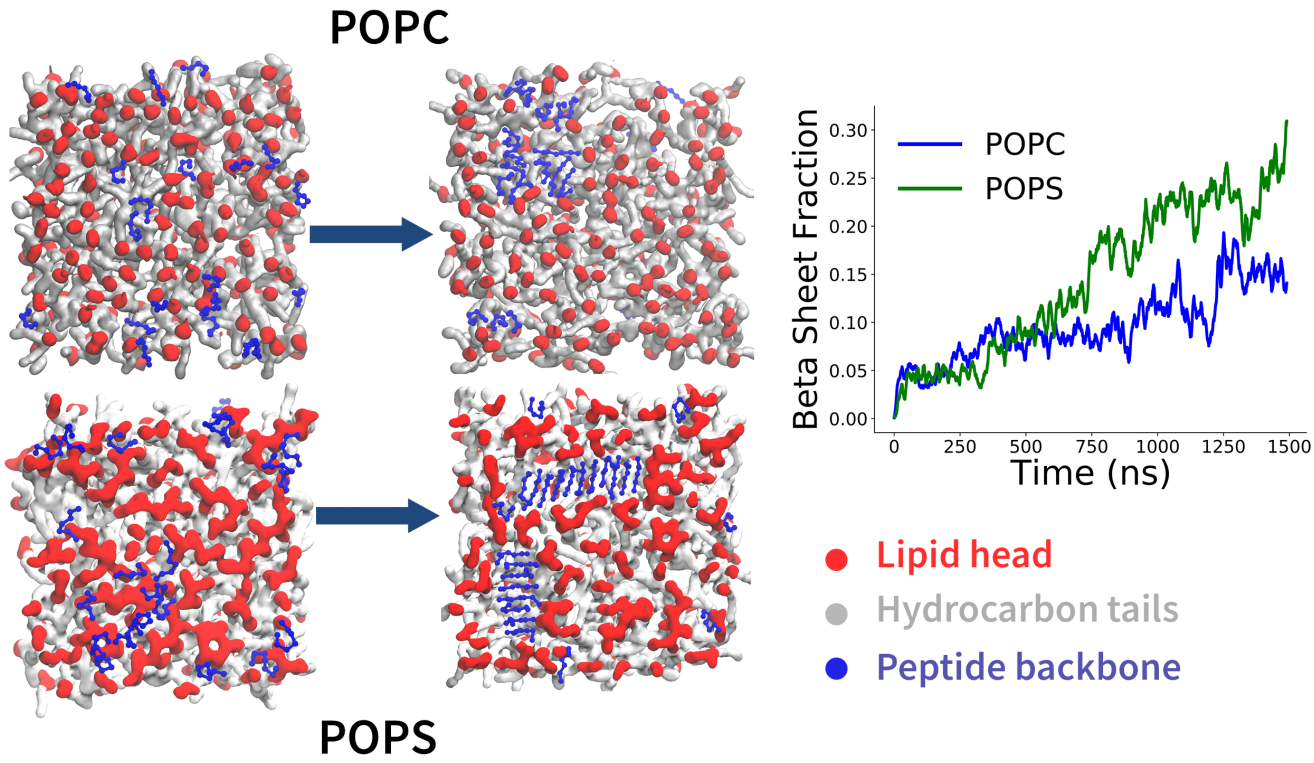

Fig. 4 Aβ 16-22 aggregation in presence of zwitterionic and anionic membranes. *Right* - The variation of beta sheet content over time. Reproduced from Sahoo *et. al.*[99] with permission from the PCCP Owner Societies.

aggregations was higher in POPS (Figure 4). The relatively higher compressibility coefficient of POPS membrane forces a more elongated conformation on peptides compared to U/O like structures in POPC membranes, thus exposing peptide backbone to more peptide-peptide contacts, resulting in higher beta sheet content.

Several common phenomena emerge from these simulations that are well supported by previous experimental studies. To summarize, charge on lipid headgroups play a crucial role in Aβ peptide-membrane binding, local environmental alterations, peptide aggregation and insertion. While peptide self-association is promoted by the presence of anionic lipid headgroups, membrane insertion and potential membrane disruption is higher for zwitterionic membranes[106]. Recent circular dichorism and Thioflavin-T studies have reported faster growth of ordered Aβ 16-28 aggre-

gations in presence of anionic vesicles[107]. Neutron diffraction studies by Dante *et. al.* have also suggested an increased intercalcation of Aβ 25-35 in anionic membranes[96]. Aggregate sizes also control the stability of membrane-inserted amyloid species, with smaller oligomers, which have been hypothesized as the more toxic entities, deemed more stable than larger fibrils. Cholesterol, sphingomyelin and gangliosides modulates peptide-lipid association by either changing lipid bilayer's physical properties (*e.g.* lipid rafts) or by introducing changes to lipid surface chemistry. Although the protective role of cholesterol is highlighted in previously mentioned simulation studies, the complex interplay between membrane's cholesterol and ganglioside concentrations and their mutually cooperative relationship in amyloid formation has not been investigated through simulations. Recent experimental investigations are also focusing on impact of Aβ on membrane dynamics. This is an exciting direction that can benefit from computational modelling.

In-silico studies have been used to evidence experimental observations in a much controlled environment and describe nanoscale interactions, essential for macroscopic features. An increasing number of studies are exploiting this synergy with computation to explain and direct experimental studies[81,92,108]. Computational and experimental studies of Aβ peptides in solution have reported a wide diversity of aggregate structures with atomistic resolution. In future, studies should be directed at understanding extensive bio-mechanical modes of these oligomer-enabled membrane disruption. Although divalent metal ions are instrumental in membrane interaction and peptide aggregation[26,109], due to absence of appropriate accurate non-polarizable forcefields, computational studies into divalent ion induced aggregation pathways is missing. In addition, computational studies should also be directed towards molecular level interactions that result in calcium dysregulation as a consequence to amyloid membrane pores. Recent computational advances in this direction such as fixed non-bonded interactions (Nbfix)[110] and scaled charges[111] to reproduce polarization in a mean-field ansatz can be helpful.

3 Parkinson's Disease - α-synuclein

Commonly located along synaptic terminals, α-synuclein (α-syn), a 140 amino acid residue long intrinsically disordered peptide (IDP) has been neuro-pathologically linked to Parkinson's disease[112–114]. Unlike Aβ peptide aggregates which selectively impact astrocytic plasma membrane, α-syn oligomers have been shown as non-selective to membranes and cells. But, both Aβ and α-syn follow common modes of pathogenesis — membrane disruption leading to calcium dysregulation and production of reactive oxygen species resulting in mitochondrial depolarization[115]. While α-syn is disordered in cytosolic state, it adopts a more ordered α-helical form in a lipidic environment[114,116]. This lipid-association also promotes misfolding and subsequent aggregation into multiple structurally dis-similar transient β-sheet rich fibrillar structures. These structures are primary constituents of Lewy-bodies that are hallmarks of PD. α-syn can be broadly categorized into three segments, N-terminal residues (1-60) - lipid-binding motifs, the central hydrophobic non amyloid component (61-95) responsible for α-syn aggregation and unstructured negatively charged C terminus (96-140) that are primary metal and peptide binding sites. In addition, there are seven imperfect eleven residue long repeat sequences with mostly conserved KTKEGV hexamer motifs (Figure 5), spread over N-terminal and NAC domains, that contribute to α-helical structures and lipid-binding. The lipid-induced conformational transition into α-helical structure, exposes NAC domain, increasing the overall hydrophobic surface area and promoting aggregation[114]. Increase in local peptide concentration by lipid bilayer association, has also been implicated for peptide aggregation. As with Aβ peptides, membrane composition, particularly membrane charge plays a critical role in modulating α-syn-membrane interactions, with interactions between negatively charged lipid group and positively charged lysines tethering the peptide onto the membrane. Initial studies on peptide interaction specificity have noted a preference for membranes containing anionic lipids, with more favorable interactions between PA (Phosphatidic acid)/PI (Phosphatidylinositol)[117,118]. Investigations by confocal microscopy and atomic force microscopy have revealed that α-syn interacts with gangliosides through hydrogen bonds with sugar-alcohols[119]. In addition, lipid tail order also modulates α-syn membrane interaction, with a preference for more disordered poly-unsaturated tails, which can generate more packing defects due to loose packing[120,121]. Beyond preference for individual lipids, peptides also show a significantly increased (about 15-fold) binding affinity for membranes with higher curvature (small unilamellar vesicles) than large/giant unilamellar vesicles[117,122,123]. Membrane disruption due to α-syn oligomers, have revealed increased tubulations on membranes, compared to larger fibrils[124,125].

The primary mode of α-syn induced PD pathology is associated with flattening of membrane curvature[114]. Vesicle fusion is driven by release of curvature induced stress. The membrane distortion and flattening in presence of α-syn aggregates releases this stress, preventing fusion[126]. Initial attempts at generating membrane bound conformations of monomeric α-syn has been attempted with solution NMR and EPR studies of α-syn in association with membrane-like surfactants (SLAS - sodium lauroyl sarcosinate and SDS - sodium dodecyl sulfate)[127,128]. Jao *et. al.* presented a POPG vesicle-bound structure of α-syn, which were significantly different from structures obtained from studies using micelles, through site directed spin labelling, EPR based approaches and simulated annealing molecular dynamics[129]. More recently a combination of solid-state NMR and solution NMR were used along with small unilamellar vesicles to decipher the structure of α-syn monomer associated with the membrane. The results confirmed the three domain structure of membrane associated α helix with unstructured C-terminus[130]. Due to experimental limitations, most experiments, aimed towards predicting α-syn aggregate structures have focused on aqueous solvated α-syn.

A full atomic resolution picture and structural details of α-syn oligomers, particularly in membrane-associated forms is yet to be reliably determined from experiments. In addition, the mechanistic details of α-syn induced membrane disruption and associated PD pathology remains elusive. Many *in-silico* experiments have been attempted to bridge this gap.

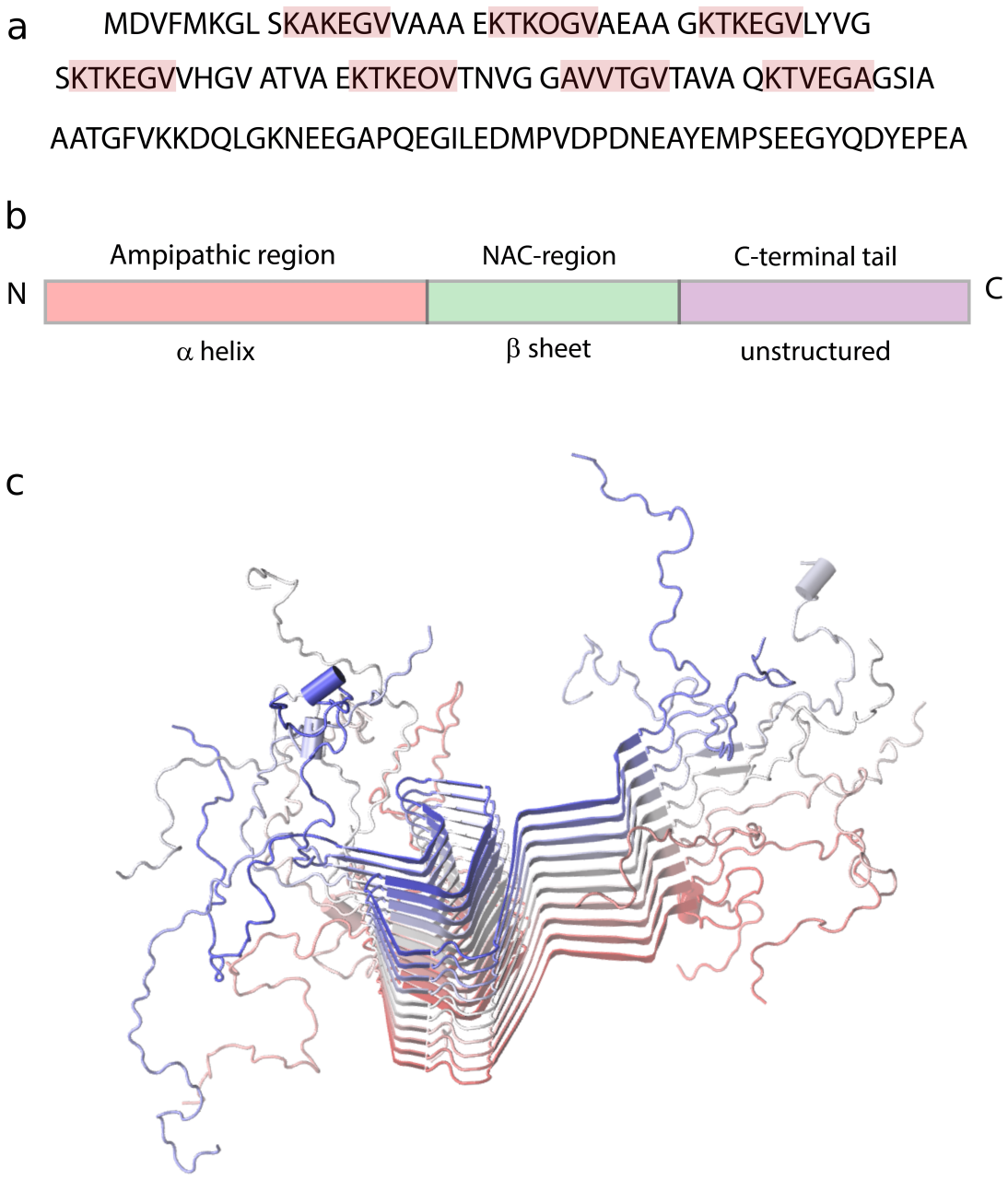

Fig. 5 a) Amino acids in α-synuclein. The shaded region presents mostly conserved KTKGEV hexamers in 11 residue imperfect repeats. b) A characteristic structure of α-syn monomer. c) A representative structure of α-syn oligomer (pdb: 2NOA) in solution. The aggregate is colored to distinguish multiple chains.

3.1 *In-silico* modelling

Submersion of α-syn 1-15 into model bilayer made from POPC/POPA (1:1) was investigated with C36 (lipids), CHARMM22 (peptides) and TIP3P (water) forcefields using umbrella sampling[131]. Simulations reveal hydrophobic residues — M1, W4, and L8 embedded deep into bilayer and polar residues — D2, K6, S9, K10, and E13 present at bilayer surface, with L8 and S9 acting as pivot. Membrane thinning due to α-syn 1-15 has also been reported. Garten *et. al.* used lipid bilayer simulations with CHARMM36 forcefield to present a molecular understanding of higher affinity of α-syn for DPhPC — 1,2-diphytanoyl-sn-glycero-3-phosphocholine compared to DOPC[132]. They observed an increase in packing defects which exposes the peptide hydrophobic patch to the bilayer surface in DPhPC compared to DOPC, which can promote peptide-membrane interactions. Vermaas *et. al.* simulated α-synuclein membrane association and peptide conformational transition using highly mobile membrane-mimetic model (HMMM) of PC/PS with CHARMM36 lipid and CHARMM27 protein forcefields[133]. The simulations could capture a transition from an initial broken-

helix state to a semi-extended helix state, aided by presence of PS lipids at the inner-edge of peptides. The study reported a highly variable peptide insertion into the bilayer. Tsigenly *et. al.* used membrane contact surface prediction and molecular simulations to categorize membrane associated oligomers as "propagating" — support addition of peptide-monomers to oligomers and "non-propagating" — do not support spontaneous oligomer growth[134]. This propagated-docking generated pentamers and hexamers, with ring like structures similar to membrane pores. The authors also found that β-syn, a non-pathogenic member of synuclein family could inhibit propagating oligomers by binding to it. Perlmutter *et. al.* suggested screening of negative-charged, acidic lipid headgroups by α-syn leading to flattening of curved membrane using simulations of α-syn bound to SDS micelles and DOPS membranes[135]. In addition, their analyses of α-syn familial mutants suggest an array of destabilizing peptide-lipid interactions in A30P mutants, threonine-based and lysine-based stabilizing interactions in A53T and E46K mutants.

In addition to atomistic simulations, coarse grained MD with MARTINI forcefield[47] has been used to study peptide associated membrane deformations. These coarse grained simulations are particularly advantageous in capturing the large-scale membrane modulating behavior of α-syn, while preserving molecular specificity of peptides and lipids. Braun *et. al.* studied generation of membrane curvature due to presence of α-syn peptides in an extended α-helix-turn-α-helix state[136]. The presence of α-syn induced negative gaussian curvature — associated with fusion and fission states and positive mean curvature on lipid bilayer composed of POPC and POPS. The authors proposed that interactions between peptides on membranes can be cast as interactions between intrinsic local curvature fields. A comparative analysis of POPG membrane binding and remodeling capacity of α-syn 1-78 and α-syn 1-100 was probed using MARTINI forcefield[137]. The decrease in amino acids primarily from NAC region, reduces membrane association membrane deformation. MARTINI simulations with DPPC SUVs with α-syn at a ratio of 200:1 presented lowered surface tension and increased membrane undulations due to α-syn membrane associations[138]. Multiple simulations with varying lipid content and fluorescence correlation spectroscopy were implemented to study tubulations and peptide induced curvature. Membrane disruption/tubulations, promoted by increased binding affinity of highly anionic POPG membranes was higher than POPC/POPG membranes[139]. The analyses also suggest anti-alligned interdigitation between opposing monolayers during tubulations. Tsigelny *et. al.* used implicit solvent MD to enumerate distinct amino acid zones for α-syn wild type and familial mutant membrane contacts and amino acids (L38, V48, V49, Q62, and T64) that promote inter-peptide interaction[140]. They also reported an enhanced propensity for annular oligomers in E57K, A53T, and H50Q mutants compared to E46K, E35K, wild-type and A30P.

These results provide an overview of recent computational advances in our understanding of α-syn membrane interactions. In agreement with experimental results, and similar to Aβ, α-syn also interacts strongly anionic membranes. But, in contrast to Aβ peptides, where membrane disruption is more pronounced in disordered-zwitterionic membranes, membrane tubulations in presence of α-syn is higher in model anionic membranes. A concurring theme in both experimental and computational literature is the modulation of local membrane curvature in presence of α-syn. While computational simulations have primarily focused on single peptide stability and membrane disruption, conformational changes (both structural and kinetic effects) in α-syn due to membrane association is yet to be investigated. Similar to Aβ peptides, experiments have uncovered the role of cholesterol and gangliosides in driving α-syn insertion and pore formation. Further *in-silico* investigations into this can uncover atomic micro-interactions and associated kinetics of this process. Recent computational and experimental studies (Cryo-EM and Solid-state NMR) have uncovered multiple atomic resolution structures of α-syn fibrils, suggesting extensive structural polymorphism[141–144]. Computational investigations on the effect of such peptide aggregations on membrane stability can be quite instructive.

4 Huntington's disease - Huntingtin protein (htt)

Another neurodegenerative disease that involves progressive amyloid deposition and associated membrane disruption is Huntington's disease[145–147]. The pathogenesis of dominantly inherited Huntigton's disease is linked to fibrillar nano-scale deposits of huntingtin protein (htt). The mutant genes encode variants of htt protein with anomalous expanded homopolymeric PolyQ sequences that aid the aggregation process. While the flanking amino acid residues, particularly, the first 17 N-terminal amino acid residues (Nt17) modulate aggregation behavior and lipid binding by formation of amphipathic alpha helix, the length of PolyQ tract directly participates in aggregation and generation of a variety of aggregate species — oligomers and larger fibrillar structures. Several reports indicate htt protein interacts with membrane, either through intracellular vesicular transport, or by association with Endoplasmic reticulum and Golgi apparatus. In addition, the pathogenesis of Huntington's disease is hypothesized to proceed through mitochondrial dysfunction. But the membrane interactions of htt and polyQ deposits have not been fully characterized.

Similar to Aβ and α-synuclein, both membranes and oligomers are affected by htt-membrane association. Solution AFM studies have reported oligomeric and fibrillar deposits over mica surface[148,149]. Studies have demonstrated an alteration in htt alpha helical content in presence of POPC and POPC/POPS SUVs[150]. AFM studies with TBLE suggests local alterations of bilayer compressibility on interaction with htt oligomers[151]. Amorphous structures and oligomers of htt exon 1 was reported as the dominant aggregate species in lipid-liquid interface with significant dependence on the length of polyQ sequence. Investigations by Chaibva et.al. suggested an enhanced peptide (Nt17Q35P10KK) binding and aggregation propensities with increase in membrane curvature[152]. They pointed at lipid packing defects associated with membrane curvature as possible mechanism for peptide binding, which then increases local peptide density to promote subsequent aggregation.

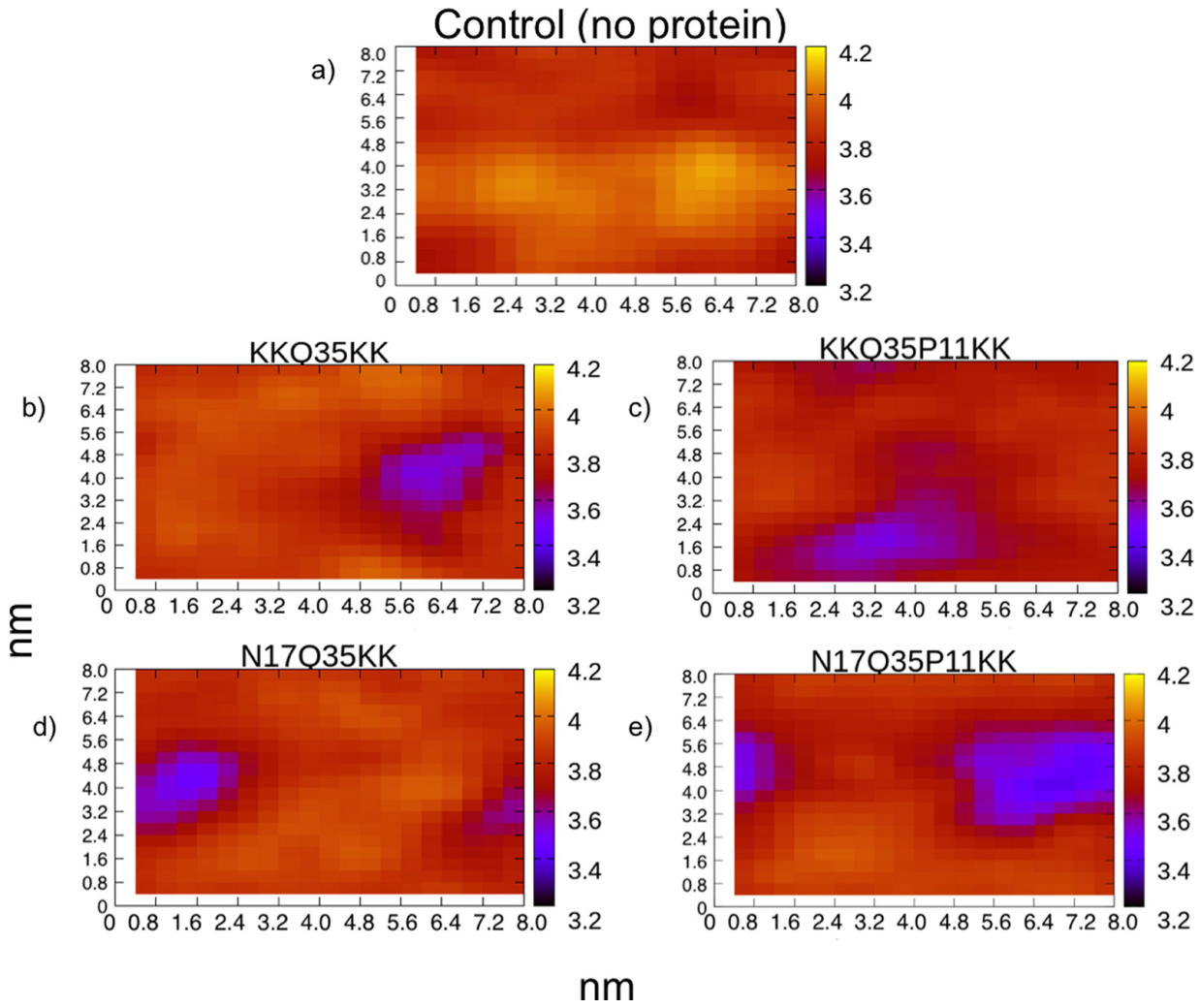

Fig. 6 Thickness of membrane of control system and different peptide variants. Reprinted with permission from A. Nagarajan, S. Jawahery and S. Matysiak, The Journal of Physical Chemistry B, 2014, 118, 6368 - 6379.

Our group probed the importance of flanking amino acid sequences (KKQ35KK, KKQ35P11KK, Nt17Q35KK, Nt17Q35P11KK) to polyQ chain that modulates membrane (single component DOPC membrane) association and potential implications of such membrane association, using atomistic simulations[153]. The simulations revealed that a majority of peptide sequences, except for KKQ35P11KK, adopted a higher β sheet content suggesting a start of fibril formation. In addition, a significant membrane thinning was reported for Nt17Q35P11KK (Figure 6), where the poly-proline sequence that generally impedes membrane association reversed its effect in presence of Nt17. Atomistic studies investigated the stability and orientation of Nt17Q20 peptide in presence of POPE model membranes[154]. Nt17 peptide arranges into stable α helix parallel to membrane surface with Leu and Phe at the hydrophobic core and Ser, Thr, Lys and Glu at polar headgroup. The polyQ sequence is positioned in solution to increase accessibility for oligomerization. Additionally, increase in polyQ sequence was not able to significantly change the behaviour of Nt17. The acetylation of Nt17 lysines (K6, K9 and K15) results in significantly reduced fibrillation rates in solution, forming globular aggregations and a decreased membrane disruption than wild type[155]. Atomistic approaches were used to investigate molecular interaction promoting this phenomena. Although there was a decrease in stabilizing interactions of phosphate groups with acetylated K and E, an increase in interaction between phosphate and polar amino acid residues was also reported.

While scarce in number, these simulations keep reiterating the importance of particular regions of htt protein in driving membrane interactions. Similar to previously established experimental observations, peptide aggregation on lipid bilayer is driven by Nt17 residues with secondary structure modifications on interaction with membranes. Atomistic interactions that drive and stabilize this membrane associated structure and the importance of N-terminal Lysines at promoting aggregation was reported. Due to significantly larger size of peptide sequence for htt, studies of peptide aggregation has not been attempted yet. Although, some coarse grained simulations have been used to characterize peptide htt aggregation landscape, CG studies of htt-membrane interaction has not been attempted yet. Therefore, in future more

studies should attempt to verify membrane disruption and membrane induced oligomerization pathways presented from experimental observations and predictions from monomer-based simulations.

5 Non-specific simulations to study membrane-assisted aggregation

Many non-specific (no specificity in molecular modeling of amino acids and lipid types) coarse grained simulations of membrane assisted peptide aggregation have been attempted to understand the general physics of peptide aggregation in presence of membranes. These simulations use a reduced resolution description of a system, leading to lower degrees of freedom and sampling of longer length and time scales.

Friedman *et. al.* used a ultra-coarse grained 10 bead peptide model — four partially charged generating dipoles, four hydrophilic and two hydrophobic beads, with a 3 bead lipid model — one hydrophilic and two hydrophobic, to study the impact of peptide amyloidogenicity on membrane/vesicle permeability[156]. First, the peptide monomeric conformational landscape was divided into amyloid competent state (β) with parallel aligned dipoles pependicular to fibril axis and amyloid protected state (π) with all conformations not in β state. Amyloidogenic property is defined by difference in energy between β and π states, which can be modulated by varying peptide dihedral angles. The simulations presented differential behaviorof this amyloidogenic and non-amyloidogenic peptides in presence of lipid vesicles. While highly amyloidogenic peptides aggregate into fibrillar structures on vesicles, lipid vesicles can effectively hinder the growth of non-amyloidogenic sequences. Moreover their research also showed that growth of amyloid fibrils rather than mature fibrillar aggregates cause membrane disruption. More recently, Morriss-Andrews *et. al.* parametrized a simpler three bead per residue peptide model and a five-bead per residue lipid model to study membrane induced beta sheet formation and characterize peptide aggregate absorption pathways. Their research also categorized several similarities in peptide aggregate morphology and dynamics between membranes and solid surface[157]. While peptides adopt a β sheet rich parallel orientation on top of both types of surfaces, the aggregates on membranes are highly dynamic and can reverse kinetics in response to membrane's oscillation. In addition, the authors also observed a lipid reorganization into hexagonal lattice structures around peptide aggregates, an increased bending modulus and dampening of fluctuations in membrane thickness with their model. Our lab studied aggregation of model peptide — Elastin-like octapeptides $(GV)_4$ in presence of hydrophobic (hexadecane)-hydrophilic (water) interface with WEPPRO[158]. The aggregation behavior was dominated by hydrophobic interactions in solution whereas dipole interaction played a more significant role in β sheet rich aggregate structure formation at the polar-hydrophobic interface. The presence of an interface resulted in a faster aggregation into a final ordered conformation and a decrease in lag phase before ordered aggregation compared to simulations in aqueous systems.

6 Concluding Remarks

Long length and time scales pose significant challenge for standard molecular dynamics studies involving peptide aggregation in presence of membranes. A better sampling of molecular pathways for the process can be achieved through emerging non-traditional advanced techniques such as Replica exchange molecular dynamics[159], parallel tempering in the well-tempered ensemble[160], metadynamics (traditional[161,162], bias-exchange[163] and solute tempering[164]). Most simulation based studies using advanced sampling techniques have focused on self-association in solution due to inherent computational simplicity. Although some advanced sampling studies have been attempted to study systems involving membranes and aggregating peptides, more effort is needed along that direction. It should be noted that although advanced sampling techniques generate sufficient convergence of multiple conformations, many details of the system dynamics are lost.

Coarse grained simulations, which capture both structure and dynamics simultaneously can be an viable alternative, with a definite trade-off of accuracy to increase computational efficiency. Similar to most advanced sampling methods, most novel coarse graining techniques with peptide sequence specificity in present literature — OPEP[165], AWSEM-MD[166] and PRIME20[167] can only be applied to study peptide oligomerization in solution, due to absence of any compatible lipid model. While other simulation forcefields such as MARTINI which has been used to study peptide aggregation and membrane-peptide systems, they cannot study peptide structural transitions which are ubiquitous in membrane assisted peptide oligomerization. Although recently developed coarse graining schemes which employ partial charges to reproduce structural polarization — WEPMEM-WEPPRO[99,100,104,105,158], do capture unbiased transition to peptide secondary structures, extensive research needs to be done on their reliability and transfer-ability to longer peptide sequences. Along this direction, molecular dynamics simulations with varying resolution, which involves mapping from atomistic to coarse grained scales and reverse over multiple iterations can provide desired accuracy (not accessible from purely coarse grained simulations), while maintaining extensive sampling.

Many controversies and variations in results from traditional atomistic computational studies can be directly attributed to forcefield accuracy. A recently published report compared oligomerization of Aβ 16-22 and its three mutants F19V, F20V anf F19L across five different forcefields — Gromos54a7, OPLS-AA, AMBER03WS, CHARMM22, and AMBER99SB-ILDN[168]. This study presented quite disparate results with aggregation structures and kinetics. The authors suggested using a "consensus forcefield" approach[169,170] in which simulations of a particular system are performed across multiple forcefields to generate consensus results. A similar work from this group applied multiple forcefields (OPLS, AMBER99SB, AMBER99SB-ILDN, AMBER99SBILDN-NMR and CHARMM22) to study full length Aβ 1-42 monomeric conformations and matched that to observations from NMR[171]. They have reported that CHARMM22 provides the best match with local NMR observables. Another re-

search compared dimerization of Aβ 16-22 across multiple forcefields and clustered the forcefields on the basis of their predicted structural and kinetic properties[172]. These authors suggested to use AMBER99-ILDN, AMBER14SB, CHARMM22, CHARMM36, and CHARMM36m. Similar comparisions across lipid forcefields has suggested that no single forcefield could reliably capture all possible membrane properties. These results present significant pressure to develop more accurate forcefields that can capture highly dynamic nature of IDP peptides and structural properties of membranes. Recent advancements in development and validation of lipid forcefields have been outlined by Leonard *et. al.*[173].

Individually, both peptide and lipid forcefields have been parametrized to reproduce ab-initio data, structural information from experiments and thermodynamic properties. But the dearth of experimental data for peptide-lipid systems has made refinement and validation of peptide-lipid forcefields difficult. A recent assessment of atomistic protein-lipid forcefields — GROMOS54a7, CHARMM36, Amber14sb/Slipids and Amber14sb/Lipid14 using different experimentally verifiable observables showed that CHARMM36 forcefield has the highest correlation with experiments[174]. As no current classical molecular forcefield can be hailed the best, computational scientists should focus on how predictive a particular forcefield is regarding available experimental observations about that particular chemical system. In addition, considering the highly non-equilibrium nature of protein-membrane partitioning, membrane assisted aggregation and protein induced membrane disruption, forcefields need to be parametrized using dynamical experiments, beyond current attempts to model structural properties. Further, the inaccurate representation of ionic forcefield has continuously plagued the molecular simulation community. Research efforts towards developing efficient polarizable or/and multi-body ion potentials is instrumental in simulating accurate cellular environments. Beyond electrostatics, it is crucial to capture long-range Lennard Jones (LJ) potential to capture transitions from solution to membrane. Similar to electrostatic potential, recent research efforts are focusing on representing long range LJ by a particle-mesh-Ewald (PME) method, which necessitates further parametrization. More recently, machine learning techniques have been applied for appropriate parametrization of forcefields, which opens unique possibilities. On a separate note, polarizable forcefields (AMBER ff02, CHARMM Drude, AMOEBA, etc.), which are generally more accurate suffer from high computational complexity and are significantly slower than non-polarizable ones. Therefore, polarizable forcefields have not been used to study complex peptide membrane associations.

Moreover, there is a need to simulate peptide aggregation in a more cell-like representative crowded environments. Local environments and many long length and time scale processes are intricately tangled to result in peptide aggregation, particularly in presence of highly diverse lipidic environments which may be composed of around 1000 types of lipid molecules and multiple embedded proteins. This astounding complexity poses a problem of how large and diverse should a simulation system be to appropriately capture interesting dynamics in a heterogeneous and crowded environment. Simulations of this scale involves molecular communication over long length/time scales. owing to the hierarchical nature of biological systems, development of techniques to accurately communicate across multiple scales, while preventing errors from propagating, is essential. Although, with current computational machinaries, it is impossible to capture such time and length scales by conventional molecular dynamics, over the next decade, it might be possible to study peptide aggregation processes over minimal representative cells, particularly with coarse grained representation. Recent efforts towards creation of a representative plasma membrane using MARTINI forcefield is a significant step towards this[175]. Simulations along this direction can provide significant insights about accurate pathogenesis of several neurodegenerative diseases and present pathways for therapeutic interventions.

With the progressive increase in computational investigations into biomolecular systems, we are presented with an urgent need to follow a more open-source approach towards data and protocols to generate reproducible and avoid erroneous results. Although, we are still far from a comprehensive picture of peptide-induced amyloid formation, molecular simulation certainly can be an effective tool to assist experimental investigations. With advancements in statistical theories, leading up to novel simulation techniques and molecular forcefields, and continued growth in high performance computing infrastructure, molecular simulations will continue to unravel mysteries presented by these complex processes.

Acknowledgement

This research was supported by the National Science Foundation under the Grant CHE-1454948 and through XSEDE resources provided by the Texas Advanced Computing Center (TACC) under the grant number TG-MCB120045.

References

1 C. A. Ross and M. A. Poirier, *Nat. Med.*, 2004, **10**, S10–S17.
2 T. R. Jahn, O. S. Makin, K. L. Morris, K. E. Marshall, P. Tian, P. Sikorski and L. C. Serpell, *J. Mol. Biol.*, 2010, **395**, 717–727.
3 M. Verma, A. Vats and V. Taneja, *Ann Indian Acad Neurol*, 2015, **18**, 138–45.
4 F. G. De Felice and S. T. Ferreira, *Cell. Mol. Neurobiol.*, 2002, **22**, 545–63.
5 W. L. Klein, G. A. Krafft and C. E. Finch, *Trends Neurosci.*, 2001, **24**, 219–24.
6 D. M. Walsh and D. J. Selkoe, *J. Neurochem.*, 2007, **101**, 1172–1184.
7 H. LIN, R. BHATIA and R. LAL, *FASEB J.*, 2001, **15**, 2433–2444.
8 S. Butterfield and H. Lashuel, *Angew. Chem.*, 2010, **49**, 5628–5654.
9 N. Arispe, H. B. Pollard, E. Rojas, R. Azimova, D. Ng, B. Frangione, B. Kagan, J. Ghiso and R. Lal, *Proc. Natl. Acad. Sci. U.S.A.*, 1993, **90**, 10573–7.
10 T. R. Serio, A. G. Cashikar, A. S. Kowal, G. J. Sawicki, J. J. Moslehi, L. Serpell, M. F. Arnsdorf and S. L. Lindquist, *Sci-*

ence, 2000, **289**, 1317–1321.
11 I. V. J. Murray, M. E. Sindoni and P. H. Axelsen, *Biochemistry*, 2005, **44**, 12606–13.
12 M. J. Volles, S. J. Lee, J. C. Rochet, M. D. Shtilerman, T. T. Ding, J. C. Kessler and P. T. Lansbury, *Biochemistry*, 2001, **40**, 7812–9.
13 M. Michikawa, J.-S. Gong, Q.-W. Fan, N. Sawamura and K. Yanagisawa, *J. Neurosci.*, 2001, **21**, 7226–7235.
14 C. R. Flach, J. W. Brauner, J. W. Taylor, R. C. Baldwin and R. Mendelsohn, *Biophys. J.*, 1994, **67**, 402–10.
15 V. Koppaka and P. H. Axelsen, *Biochemistry*, 2000, **39**, 10011–6.
16 L. Liu, H. Komatsu, I. V. Murray and P. H. Axelsen, *J. Mol. Biol.*, 2008, **377**, 1236–1250.
17 J. Homola, *Chem. Rev.*, 2008, 462–493.
18 H. Mozsolits and M.-I. Aguilar, *Biopolymers*, 2002, **66**, 3–18.
19 M. Winterhalter, *Curr. Opin. Colloid Interface Sci*, 2000, **5**, 250–255.
20 M. C. Lin, T. Mirzabekov and B. L. Kagan, *J. Biol. Chem.*, 1997, **272**, 44–7.
21 M. J. O. Widenbrant, J. Rajadas, C. Sutardja and G. G. Fuller, *Biophys. J.*, 2006, **91**, 4071.
22 T. Hamada, M. Morita, Y. Kishimoto, Y. Komatsu, M. Vestergaard and M. Takagi, *J Phys Chem Lett*, 2010, **1**, 170–173.
23 E. Sparr, M. F. Engel, D. V. Sakharov, M. Sprong, J. Jacobs, B. de Kruijff, J. W. Höppener and J. Antoinette Killian, *FEBS Lett.*, 2004, **577**, 117–120.
24 M. Bokvist, F. Lindström, A. Watts and G. Gröbner, *J. Mol. Biol.*, 2004, **335**, 1039–49.
25 C. C. Curtain, F. Ali, I. Volitakis, R. A. Cherny, R. S. Norton, K. Beyreuther, C. J. Barrow, C. L. Masters, A. I. Bush and K. J. Barnham, *J. Biol. Chem.*, 2001, **276**, 20466–20473.
26 C. C. Curtain, F. E. Ali, D. G. Smith, A. I. Bush, C. L. Masters and K. J. Barnham, *J. Biol. Chem.*, 2003, **278**, 2977–82.
27 J. D. Knight and A. D. Miranker, *J. Mol. Biol.*, 2004, **341**, 1175–1187.
28 M. Biancalana, K. Makabe, A. Koide and S. Koide, *J. Mol. Biol.*, 2009, **385**, 1052–1063.
29 L. A. Munishkina and A. L. Fink, *Biochim Biophys Acta Biomembr*, 2007, **1768**, 1862–1885.
30 L. Qiu, A. Lewis, J. Como, M. W. Vaughn, J. Huang, P. Somerharju, J. Virtanen and K. H. Cheng, *Biophys. J.*, 2009, **96**, 4299–4307.
31 K. Berthelot, C. Cullin and S. Lecomte, *Biochimie*, 2013, **95**, 12–19.
32 R. O. Dror, R. M. Dirks, J. P. Grossman, H. Xu and D. E. Shaw, *Annu Rev Biophys*, 2012, 429–52.
33 B. A. Merchant and J. D. Madura, *Annual Reports in Computational Chemistry*, 2011, **7**, 67–87.
34 M. J. Abraham, T. Murtola, R. Schulz, S. Páll, J. C. Smith, B. Hess and E. Lindahl, *SoftwareX*, 2015, **1-2**, 19–25.
35 B. R. Brooks, C. L. Brooks, A. D. Mackerell, L. Nilsson, R. J. Petrella, B. Roux, Y. Won, G. Archontis, C. Bartels, S. Boresch, A. Caflisch, L. Caves, Q. Cui, A. R. Dinner, M. Feig, S. Fischer, J. Gao, M. Hodoscek, W. Im, K. Kuczera, T. Lazaridis, J. Ma, V. Ovchinnikov, E. Paci, R. W. Pastor, C. B. Post, J. Z. Pu, M. Schaefer, B. Tidor, R. M. Venable, H. L. Woodcock, X. Wu, W. Yang, D. M. York and M. Karplus, *Journal of Computational Chemistry*, 2009, **30**, 1545–1614.
36 J. C. Phillips, R. Braun, W. Wang, J. Gumbart, E. Tajkhorshid, E. Villa, C. Chipot, R. D. Skeel, L. Kalé and K. Schulten, *Journal of Computational Chemistry*, 2005, **26**, 1781–1802.
37 I. T. Todorov, W. Smith, K. Trachenko and M. T. Dove, *Journal of Materials Chemistry*, 2006, **16**, 1911.
38 J. A. Maier, C. Martinez, K. Kasavajhala, L. Wickstrom, K. E. Hauser and C. Simmerling, *J. Chem. Theory Comput.*, 2015, **11**, 3696–3713.
39 C. J. Dickson, B. D. Madej, Å. A. Skjevik, R. M. Betz, K. Teigen, I. R. Gould and R. C. Walker, *J. Chem. Theory Comput.*, 2014, **10**, 865–879.
40 R. B. Best, X. Zhu, J. Shim, P. E. M. Lopes, J. Mittal, M. Feig and A. D. MacKerell, *J. Chem. Theory Comput.*, 2012, **8**, 3257–3273.
41 R. W. Pastor and A. D. MacKerell, *J. Phys. Chem. Lett.*, 2011, **2**, 1526–1532.
42 J. B. Klauda, V. Monje, T. Kim and W. Im, *J. Phys. Chem. B*, 2012, **116**, 9424–9431.
43 C. Oostenbrink, A. Villa, A. E. Mark and W. F. Van Gunsteren, *J. Comput. Chem.*, 2004, **25**, 1656–1676.
44 S.-W. Chiu, S. A. Pandit, H. L. Scott and E. Jakobsson, *J. Phys. Chem. B*, 2009, **113**, 2748–2763.
45 W. L. Jorgensen and J. Tirado-Rives, *J. Am. Chem. Soc.*, 1988, **110**, 1657–1666.
46 D. S. M. William L. Jorgensen and J. Tirado-Rives, *J. Am. Chem. Soc.*, 1996, 11225–11236.
47 S. Y. D. P. T. Siewert J. Marrink, H. Jelger Risselada and A. H. de Vries, *J. Phys. Chem. B,*, 2007, 7812–7824.
48 L. Monticelli, S. K. Kandasamy, X. Periole, R. G. Larson, D. P. Tieleman and S.-J. Marrink, *J. Chem. Theory Comput.*, 2008, **4**, 819–834.
49 H. Braak and E. Braak, *J Neural Transm Suppl.*, 1998, **53**, 127–40.
50 C. Ballatore, V. M.-Y. Lee and J. Q. Trojanowski, *Nat. Rev. Neurosci.*, 2007, **8**, 663–72.
51 C. L. Masters, G. Simms, N. A. Weinman, G. Multhaup, B. L. McDonald and K. Beyreuther, *Proc. Natl. Acad. Sci. U.S.A.*, 1985, **82**, 4245–9.
52 G. G. Glenner and C. W. Wong, *Biochem. Biophys. Res. Commun.*, 1984, **120**, 885–90.
53 G. G. Glenner and C. W. Wong, *Biochem. Biophys. Res. Commun.*, 1984, **122**, 1131–5.
54 J. Lewis and M. G. Spillantini, *Science*, 2001, **293**, 1487–1491.
55 D. J. Selkoe, *Physiol. Rev.*, 2001, **81**, 741–766.
56 D. J. Selkoe, *Neuron*, 1991, **6**, 487–498.
57 J. Whitson, D. Selkoe, C. Cotman, L. Villa-Komaroff, M. Oster-Granite and R. Neve, *Science*, 1989, **243**, 1488–1490.

58 D. J. Selkoe, *Physiol. Rev.*, 2001, **81**, 741–766.

59 M. P. Murphy and H. LeVine, *J. Alzheimers Dis.*, 2010, **19**, 311–323.

60 E. Drolle, A. Negoda, K. Hammond, E. Pavlov and Z. Leonenko, *PLoS ONE*, 2017, **12**, e0182194.

61 J. McLaurin and A. Chakrabartty, *J. Biol. Chem.*, 1996, **271**, 26482–9.

62 K. Matsuzaki, *Biochim Biophys Acta Biomembr*, 2007, **1768**, 1935–1942.

63 E. Terzi, G. Hölzemann and J. Seelig, *J. Mol. Biol.*, 1995, **252**, 633–642.

64 P. T. Wong, J. A. Schauerte, K. C. Wisser, H. Ding, E. L. Lee, D. G. Steel and A. Gafni, *J. Mol. Biol.*, 2009, **386**, 81–96.

65 W. Gibson Wood, G. P. Eckert, U. Igbavboa and W. E. Müller, *Biochimica et biophysica acta*, 2003, **1610**, 281–90.

66 M.-A. Sani, J. D. Gehman and F. Separovic, *FEBS Lett.*, 2011, **585**, 749–754.

67 T. Kowalewski and D. M. Holtzman, *Proc. Natl. Acad. Sci. U.S.A.*, 1999, **96**, 3688–93.

68 M. R. Nichols, M. A. Moss, D. K. Reed, J. H. Hoh and T. L. Rosenberry, *Microsc. Res. Tech.*, 2005, **67**, 164–174.

69 C. E. Giacomelli and W. Norde, *Biomacromolecules*, 2003, 1719–26.

70 S. L. Gras, *Advances in Chemical Engineering*, 2009, **35**, 161–209.

71 J. J. Kremer and R. M. Murphy, *J. Biochem. Biophys. Methods*, 2003, **57**, 159–169.

72 R. Kayed, Y. Sokolov, B. Edmonds, T. M. McIntire, S. C. Milton, J. E. Hall and C. G. Glabe, *J. Biol. Chem.*, 2004, **279**, 46363–6.

73 Y. Shai, *Biochim Biophys Acta Biomembr*, 1999, **1462**, 55–70.

74 M. A. Barrett, M. Trapp, W. Lohstroh, T. Seydel, J. Ollivier, M. Ballauff, N. A. Dencher and T. Hauß, *Soft Matter*, 2016, **12**, 1444–1451.

75 A. Buchsteiner, T. Hauß and N. A. Dencher, *Soft Matter*, 2012, **8**, 424–429.

76 D. K. Rai, V. K. Sharma, D. Anunciado, H. O'Neill, E. Mamontov, V. Urban, W. T. Heller and S. Qian, *Sci. Rep*, 2016, **6**, 30983.

77 C. H. Davis and M. L. Berkowitz, *Proteins*, 2010, **78**, 2533.

78 S. T. Ngo, H. M. Hung, K. N. Tran and M. T. Nguyen, *RSC Advances*, 2017, **7**, 7346–7357.

79 E. G. Marklund, M. T. Degiacomi, C. V. Robinson, A. J. Baldwin and J. L. Benesch, *Structure*, 2015, **23**, 791–799.

80 H. Jang, F. T. Arce, S. Ramachandran, R. Capone, R. Azimova, B. L. Kagan, R. Nussinov and R. Lal, *Proc. Natl. Acad. Sci. U.S.A.*, 2010, **107**, 6538–43.

81 H. Ahyayauch, M. Raab, J. Busto, N. Andraka, J.-L. Arrondo, M. Masserini, I. Tvaroska and F. Goñi, *Biophys. J.*, 2012, **103**, 453–463.

82 A. Brown and D. Bevan, *Biophys. J.*, 2016, **111**, 937.

83 J. V. Rushworth and N. M. Hooper, *Int J Alzheimers Dis*, 2011, **2011**, 1–14.

84 C. H. Davis and M. L. Berkowitz, *J Phys Chem B*, 2009, **113**, 14480–14486.

85 C. H. Davis and M. L. Berkowitz, *Biophys. J.*, 2009, **96**, 785–797.

86 T. Hoshino, M. I. Mahmood, K. Mori and K. Matsuzaki, *J Phys Chem B*, 2013, **117**, 8085–8094.

87 C. Poojari, A. Kukol and B. Strodel, *Biochim Biophys Acta Biomembr*, 2013, **1828**, 327–339.

88 B. Strodel, J. W. L. Lee, C. S. Whittleston and D. J. Wales, *J. Am. Chem. Soc.*, 2010, **132**, 13300–13312.

89 F. Kargar, S. Emadi and H. Fazli, *Proteins*, 2017, **85**, 1298–1310.

90 J. A. Lemkul and D. R. Bevan, *Biochemistry*, 2013, 4971–4980.

91 H. Jang, L. Connelly, F. Teran Arce, S. Ramachandran, B. L. Kagan, R. Lal and R. Nussinov, *J Chem Theory Comput*, 2013, **9**, 822–833.

92 A. Khondker, R. J. Alsop, S. Himbert, J. Tang, A.-C. Shi, A. P. Hitchcock and M. C. Rheinstädter, *Scientific Reports*, 2018, **8**, 12367.

93 C. Poojari and B. Strodel, *PLoS ONE*, 2013, **8**, e78399.

94 L. Qiu, C. Buie, A. Reay, M. W. Vaughn and K. H. Cheng, *J. Phys. Chem. B*, 2011, **115**, 9795–812.

95 N. Xiang, Y. Lyu, X. Zhu and G. Narsimhan, *Phys. Chem. Chem. Phys.*, 2018, **20**, 6817–6829.

96 S. Dante, T. Hauß and N. A. Dencher, *Eur. Biophys. J.*, 2006, **35**, 523–531.

97 I. Sponne, A. Fifre, V. Koziel, T. Oster, J.-L. Oliver and T. Pillot, *FASEB J.*, 2004, **18**, 836–838.

98 J. Habchi, S. Chia, C. Galvagnion, T. C. T. Michaels, M. M. J. Bellaiche, F. S. Ruggeri, M. Sanguanini, I. Idini, J. R. Kumita, E. Sparr, S. Linse, C. M. Dobson, T. P. J. Knowles and M. Vendruscolo, *Nat. Chem.*, 2018, **10**, 673–683.

99 A. Sahoo, H. Xu and S. Matysiak, *Phys Chem Chem Phys*, 2019, **21**, 8559–8568.

100 S. J. Ganesan, H. Xu and S. Matysiak, *Phys Chem Chem Phys*, 2016, **18**, 17836–17850.

101 D. L. Mobley, D. L. Cox, R. R. Singh, M. W. Maddox and M. L. Longo, *Biophys. J.*, 2004, **86**, 3585–3597.

102 N. Liguori, P. S. Nerenberg and T. Head-Gordon, *Biophys. J.*, 2013, **105**, 899–910.

103 M. Pannuzzo, D. Milardi, A. Raudino, M. Karttunen and C. La Rosa, *Phys Chem Chem Phys*, 2013, **15**, 8940.

104 S. J. Ganesan, H. Xu and S. Matysiak, *J Phys Chem B*, 2017, **121**, 787–799.

105 S. J. Ganesan and S. Matysiak, *J Chem Theory Comput*, 2014, **10**, 2569–2576.

106 F. Hane, E. Drolle, R. Gaikwad, E. Faught and Z. Leonenko, *J. Alzheimers Dis.*, 2011, **26**, 485–494.

107 N. Sureshbabu, R. Kirubagaran, H. Thangarajah, E. J. P. Malar and R. Jayakumar, *J. Mol. Neurosci.*, 2010, **41**, 368–382.

108 J. Tang, R. J. Alsop, M. Backholm, H. Dies, A.-C. Shi and M. C. Rheinstädter, *Soft Matter*, 2016, **12**, 3165–3176.

109 T.-L. Lau, E. E. Ambroggio, D. J. Tew, R. Cappai, C. L. Masters, G. D. Fidelio, K. J. Barnham and F. Separovic, *J. Mol. Biol.*, 2006, **356**, 759–770.

110 J. Yoo and A. Aksimentiev, *Phys Chem Chem Phys*, 2018, **20**, 8432–8449.

111 T. Martinek, E. Duboué-Dijon, Š. Timr, P. E. Mason, K. Baxová, H. E. Fischer, B. Schmidt, E. PluhaÅŹová and P. Jungwirth, *J Chem Phys*, 2018, **148**, 222813.

112 L. Breydo, J. W. Wu and V. N. Uversky, *Biochimica et Biophysica Acta (BBA) - Molecular Basis of Disease*, 2012, **1822**, 261–285.

113 M. Goedert, *Nat. Rev. Neurosci.*, 2001, **2**, 492–501.

114 K. Beyer, *Cell Biochem. Biophys.*, 2007, **47**, 285–299.

115 C. G. Glabe, *Neurobiol. Aging*, 2006, **27**, 570–575.

116 D. Eliezer, E. Kutluay, R. Bussell and G. Browne, *J. Mol. Biol.*, 2001, **307**, 1061–1073.

117 W. S. Davidson, A. Jonas, D. F. Clayton and J. M. George, *J. Biol. Chem.*, 1998, **273**, 9443–9.

118 R. J. Perrin, W. S. Woods, D. F. Clayton and J. M. George, *J. Biol. Chem.*, 2000, **275**, 34393–34398.

119 Zak Martinez, Min Zhu, , Shubo Han and A. L. Fink*, *Biochemistry*, 2007, 1868–1877.

120 R. J. Perrin, W. S. Woods, D. F. Clayton and J. M. George, *J. Biol. Chem.*, 2001, **276**, 41958–62.

121 S.-i. Kubo, V. M. Nemani, R. J. Chalkley, M. D. Anthony, N. Hattori, Y. Mizuno, R. H. Edwards and D. L. Fortin, *J. Biol. Chem.*, 2005, **280**, 31664–72.

122 L. Kjaer, L. Giehm, T. Heimburg and D. Otzen, *Biophys. J.*, 2009, **96**, 2857–2870.

123 E. R. Middleton and E. Rhoades, *Biophys. J.*, 2010, **99**, 2279–2288.

124 S. Campioni, B. Mannini, M. Zampagni, A. Pensalfini, C. Parrini, E. Evangelisti, A. Relini, M. Stefani, C. M. Dobson, C. Cecchi and F. Chiti, *Nature Chemical Biology*, 2010, **6**, 140–147.

125 B. Winner, R. Jappelli, S. K. Maji, P. A. Desplats, L. Boyer, S. Aigner, C. Hetzer, T. Loher, M. Vilar, S. Campioni, C. Tzitzilonis, A. Soragni, S. Jessberger, H. Mira, A. Consiglio, E. Pham, E. Masliah, F. H. Gage and R. Riek, *Proc. Natl. Acad. Sci. U.S.A*, 2011, **108**, 4194–4199.

126 F. Kamp and K. Beyer, *J. Biol. Chem.*, 2006, **281**, 9251–9259.

127 J. N. Rao, C. C. Jao, B. G. Hegde, R. Langen and T. S. Ulmer, *J. Am. Chem. Soc.*, 2010, **132**, 8657–8668.

128 T. S. Ulmer, A. Bax, N. B. Cole and R. L. Nussbaum, *J. Biol. Chem.*, 2005, **280**, 9595–603.

129 C. C. Jao, B. G. Hegde, J. Chen, I. S. Haworth and R. Langen, *Proc. Natl. Acad. Sci. U.S.A*, 2008, **105**, 19666–19671.

130 G. Fusco, T. Pape, A. D. Stephens, P. Mahou, A. R. Costa, C. F. Kaminski, G. S. Kaminski Schierle, M. Vendruscolo, G. Veglia, C. M. Dobson and A. De Simone, *Nat Commun*, 2016, **7**, 12563.

131 C. Pfefferkorn, F. Heinrich, A. Sodt, A. Maltsev, R. Pastor and J. Lee, *Biophys. J.*, 2012, **102**, 613–621.

132 M. Garten, C. Prévost, C. Cadart, R. Gautier, L. Bousset, R. Melki, P. Bassereau and S. Vanni, *Phys Chem Chem Phys*, 2015, **17**, 15589–15597.

133 J. V. Vermaas and E. Tajkhorshid, *Biochim Biophys Acta Biomembr*, 2014, **1838**, 3107–3117.

134 I. F. Tsigelny, P. Bar-On, Y. Sharikov, L. Crews, M. Hashimoto, M. A. Miller, S. H. Keller, O. Platoshyn, J. X.-J. Yuan and E. Masliah, *FEBS J.*, 2007, **274**, 1862–1877.

135 J. D. Perlmutter, A. R. Braun and J. N. Sachs, *J. Biol. Chem.*, 2009, **284**, 7177–89.

136 A. R. Braun, E. Sevcsik, P. Chin, E. Rhoades, S. Tristram-Nagle and J. N. Sachs, *J. Am. Chem. Soc.*, 2012, **134**, 2613–2620.

137 A. R. Braun, M. M. Lacy, V. C. Ducas, E. Rhoades and J. N. Sachs, *J. Membr. Biol.*, 2017, **250**, 183–193.

138 A. Braun and J. Sachs, *Biophys. J.*, 2015, **108**, 1848–1851.

139 A. R. Braun, M. M. Lacy, V. C. Ducas, E. Rhoades and J. N. Sachs, *J. Am. Chem. Soc.*, 2014, **136**, 9962–9972.

140 I. F. Tsigelny, Y. Sharikov, V. L. Kouznetsova, J. P. Greenberg, W. Wrasidlo, C. Overk, T. Gonzalez, M. Trejo, B. Spencer, K. Kosberg and E. Masliah, *ACS Chem. Neurosci.*, 2015, **6**, 403–416.

141 M. D. Tuttle, G. Comellas, A. J. Nieuwkoop, D. J. Covell, D. A. Berthold, K. D. Kloepper, J. M. Courtney, J. K. Kim, A. M. Barclay, A. Kendall, W. Wan, G. Stubbs, C. D. Schwieters, V. M. Y. Lee, J. M. George and C. M. Rienstra, *Nature Structural & Molecular Biology*, 2016, **23**, 409–415.

142 R. Guerrero-Ferreira, N. M. Taylor, D. Mona, P. Ringler, M. E. Lauer, R. Riek, M. Britschgi and H. Stahlberg, *eLife*, 2018, **7**, year.

143 D. N. Bloch and Y. Miller, *ACS Omega*, 2017, **2**, 3363–3370.

144 B. Li, P. Ge, K. A. Murray, P. Sheth, M. Zhang, G. Nair, M. R. Sawaya, W. S. Shin, D. R. Boyer, S. Ye, D. S. Eisenberg, Z. H. Zhou and L. Jiang, *Nat. Commun*, 2018, **9**, 3609.

145 J. M. Gil and A. C. Rego, *Eur. J. Neurosci.*, 2008, **27**, 2803–2820.

146 K. B. Kegel-Gleason, *J. Huntington's Dis.*, 2013, **2**, 239–50.

147 G. Bates, *Lancet*, 2003, **361**, 1642–1644.

148 K. A. Burke, J. Godbey and J. Legleiter, *Methods*, 2011, **53**, 275–284.

149 J. Legleiter, G. P. Lotz, J. Miller, J. Ko, C. Ng, G. L. Williams, S. Finkbeiner, P. H. Patterson and P. J. Muchowski, *J. Biol. Chem.*, 2009, **284**, 21647–21658.

150 R. S. Atwal, J. Xia, D. Pinchev, J. Taylor, R. M. Epand and R. Truant, *Hum. Mol. Genet.*, 2007, **16**, 2600–2615.

151 K. A. Burke, K. M. Hensal, C. S. Umbaugh, M. Chaibva and J. Legleiter, *Biochim Biophys Acta Biomembr*, 2013, **1828**, 1953–1961.

152 M. Chaibva, K. A. Burke and J. Legleiter, *Biochemistry*, 2014, **53**, 2355–2365.

153 A. Nagarajan, S. Jawahery and S. Matysiak, *J Phys Chem B*, 2014, **118**, 6368–6379.

154 S. Côté, G. Wei and N. Mousseau, *Proteins*, 2014, **82**, 1409–1427.

155 M. Chaibva, S. Jawahery, A. W. Pilkington, J. R. Arndt,

O. Sarver, S. Valentine, S. Matysiak and J. Legleiter, *Biophys. J.*, 2016, **111**, 349–362.

156 R. Friedman, R. Pellarin and A. Caflisch, *J. Mol. Biol.*, 2009, **387**, 407–415.

157 A. Morriss-Andrews, F. L. H. Brown and J.-E. Shea, *J Phys Chem B*, 2014, **118**, 8420–8432.

158 S. J. Ganesan and S. Matysiak, *Phys Chem Chem Phys*, 2016, **18**, 2449–2458.

159 T. Okabe, M. Kawata, Y. Okamoto and M. Mikami, *Chem. Phys. Lett*, 2001, **335**, 435–439.

160 M. Bonomi and M. Parrinello, *Phys. Rev. Lett.*, 2010, **104**, 190601.

161 A. Laio and F. L. Gervasio, *Rep. Prog. Phys*, 2008, **71**, 126601.

162 A. Barducci, M. Bonomi and M. Parrinello, *Wiley Interdiscip Rev Comput Mol Sci*, 2011, **1**, 826–843.

163 C. Domene, P. Barbini and S. Furini, *J Chem Theory Comput*, 2015, **11**, 1896–1906.

164 C. Camilloni, D. Provasi, G. Tiana and R. A. Broglia, *Proteins*, 2007, **71**, 1647–1654.

165 F. Sterpone, S. Melchionna, P. Tuffery, S. Pasquali, N. Mousseau, T. Cragnolini, Y. Chebaro, J.-F. St-Pierre, M. Kalimeri, A. Barducci, Y. Laurin, A. Tek, M. Baaden, P. H. Nguyen and P. Derreumaux, *Chem. Soc. Rev.*, 2014, **43**, 4871–4893.

166 A. Davtyan, N. P. Schafer, W. Zheng, C. Clementi, P. G. Wolynes and G. A. Papoian, *J Phys Chem B*, 2012, **116**, 8494.

167 M. Cheon, I. Chang and C. K. Hall, *Proteins*, 2010, **78**, 2950–60.

168 M. Carballo-Pacheco, A. E. Ismail and B. Strodel, *J Chem Theory Comput*, 2018, **14**, 6063–6075.

169 V. Gapsys, S. Michielssens, D. Seeliger and B. L. deâĂËGroot, *Angew. Chem*, 2016, **128**, 7490–7494.

170 D. Matthes, V. Gapsys, J. T. Brennecke and B. L. de Groot, *Sci Rep*, 2016, **6**, 33156.

171 M. Carballo-Pacheco and B. Strodel, *Protein Sci.*, 2017, **26**, 174–185.

172 V. H. Man, X. He, P. Derreumaux, B. Ji, X.-Q. Xie, P. H. Nguyen and J. Wang, *J Chem Theory Comput*, 2019, **15**, 1440–1452.

173 A. N. Leonard, E. Wang, V. Monje-Galvan and J. B. Klauda, *Chem. Rev.*, 2019, **119**, 6227–6269.

174 A. Sandoval-Perez, K. Pluhackova and R. A. Böckmann, *J. Chem. Theory Comput.*, 2017, **13**, 2310–2321.

175 V. Corradi, E. Mendez-Villuendas, H. I. Ingólfsson, R.-X. Gu, I. Siuda, M. N. Melo, A. Moussatova, L. J. DeGagné, B. I. Sejdiu, G. Singh, T. A. Wassenaar, K. Delgado Magnero, S. J. Marrink and D. P. Tieleman, *ACS Cent. Sci.*, 2018, **4**, 709–717.

Computational insights into lipid assisted peptide misfolding and aggregation in neurodegeneration

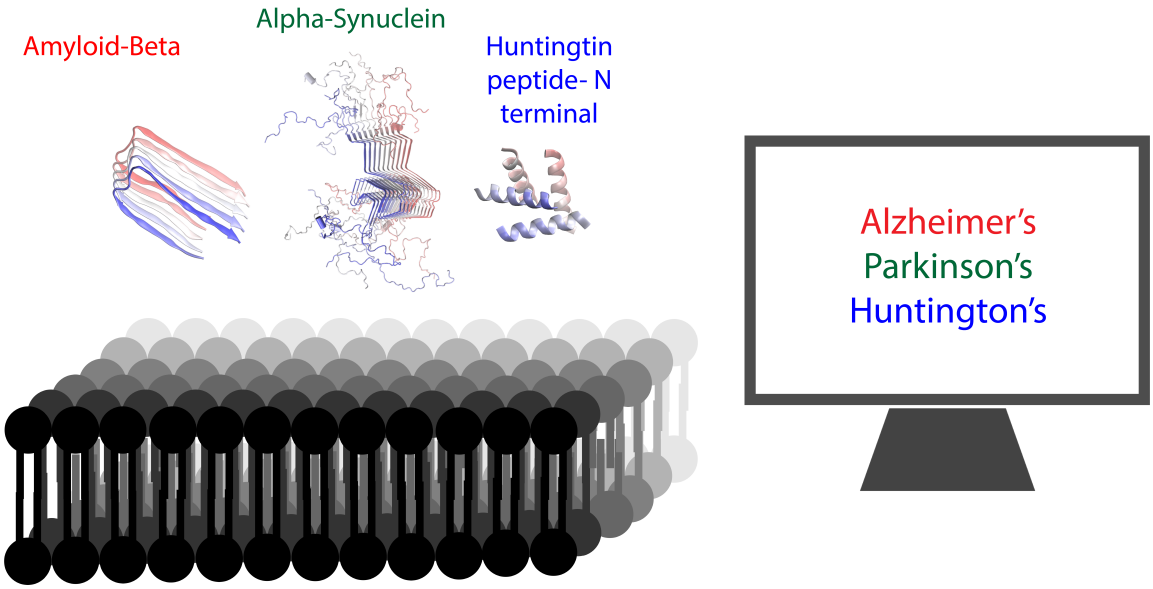

Figure 1

An overview of recent advances in computational investigation of peptide-lipid interactions in neurodegeneration — Alzheimer's, Parkinson's and Huntington's disease.